Magnetization precession induced by picosecond acoustic pulses in a freestanding film acting as an acoustic cavity

Ji-Wan Kim and Jean-Yves Bigot*

Université de Strasbourg, CNRS, Institut de Physique et Chimie des Matériaux de Strasbourg, UMR 7504, Strasbourg 67034, France

(Received 22 April 2016; revised manuscript received 17 March 2017; published 17 April 2017)

We report the magnetization dynamics excited by picosecond acoustic pulses confined in the acoustic cavity of freestanding nickel films. By detecting both sides of the sample we show that acoustic pulses moving back and forth inside the cavity efficiently control the magnetization precession. The multiple round trips of acoustic pulses, which survive for 12 bounces, enhance the amplitude of the magnetization precession by a factor of 4.5. Even though the conditions of total reflection are met in the freestanding film, the acoustic pulses have a large attenuation as compared to similar Ni films on SiO_2 substrate, for which we speculate that it is related to a stress induced by the substrate. Our results constitute a guideline for simple designs of acoustic cavities and for achieving a very large amplification of the magnetization precession angle. It is potentially useful for high-frequency magneto-optical modulators.

DOI: 10.1103/PhysRevB.95.144422

The combination of ultrafast magnetism [1] and picosecond acoustics [2] is currently an efficient approach for controlling the magnetization dynamics by avoiding thermal effects. Using picosecond acoustic pulses presents several advantages such as a high mechanical stress of GPa within a picosecond time scale [2], a long propagation distance of several millimeters with a small energy dissipation [3,4], and a large bandwidth of 0.01–1 THz with tunability [5,6]. Therefore acoustic pulses have been utilized as excitation sources in various research fields, for example, the laser emission based on acoustic resonators [7], the acoustic imaging of biocells [8], the acoustic-induced band-gap shift in semiconductors [9], magnetoacoustics [10–12], and magnetoplasmonics [13]. Moreover, to perform a magnetization switching using picosecond acoustic pulses, which is one of the ultimate objectives in applied magnetism, several configurations have been envisaged such as using various types of acoustic pulses (longitudinal and surface acoustic waves for example) [14,15], increasing the acoustic amplitude [16], or inducing a resonant motion of precession in a Bragg acoustic cavity [17].

The prerequisite for the resonant amplification of the precession is first to trap acoustic pulses in a cavity. Recently, it has been demonstrated that the acoustic standing waves generated by femtosecond laser pulses can be confined in the freestanding silicon membrane [18,19] and the propagating acoustic pulses also survived over ten round trips in the freestanding Al/Si heterostructure acting as a high-quality acoustic cavity [20]. As another technique for an acoustic cavity, the Bragg reflector has been attempted by varying the number of layers and the thickness of each layer in the superlattice structure [21]. Furthermore, the resonant motion of magnetization precession has been recently realized using a combined structure made of a ferromagnetic layer and a superlattice structure [17]. Here, as another approach of the acoustic cavity for a resonant precession of magnetization, we employ freestanding magnetic Ni films, expecting that it would be the simplest design that can overcome the acoustic impedance mismatch which usually occurs in a heterostructure composed of a magnetic and a semiconductor freestanding layer.

We performed the experiment by exciting one side of the freestanding Ni (300 nm) film with femtosecond pump pulses and detecting the differential reflectivity and magneto-optical Kerr signals on both sides using probe pulses as shown in the sketch of Fig. 1(a). The acoustic pulse with a duration of several picoseconds, which is generated by the femtosecond pump pulse (45 fs, 400 nm, 10 kHz), perturbs the elastic energy of the film and induces a precession of the magnetization via the inverse magnetostrictive effect. They are subsequently propagating back and forth in the freestanding film without loss in transmission. The probe pulses (30 fs, 800 nm, 10 kHz) measure the transient reflectivity $\Delta R(t)$ and magneto-optical polar Kerr rotation $\Delta\theta(t)$ on both the back side (BS) and front side (FS) of the film using polarization bridges and a synchronous detection scheme consisting of a reference signal on the chopped pump beam and lock-in amplifiers on the analyzed s and p probe signals. The Δ symbol for both reflectivity R and Kerr rotation θ represent the differential signals of the probes measured with and without the pump pulses. In order to separate the magnetic contribution due to the spin dynamics from the nonmagnetic one due to the charges, the processed data are obtained from measurements in the two complementary directions of the external field $H_{\text{ext}}(\varphi)$ and $H_{\text{ext}}(\varphi+\pi)$ so that $\Delta R(t) = [\Delta R_{\text{Hext}(\varphi)}(t) + \Delta R_{\text{Hext}(\varphi+\pi)}(t)]/2$ and $\Delta\theta(t) = [\Delta\theta_{\text{Hext}(\varphi)}(t) - \Delta\theta_{\text{Hext}(\varphi+\pi)}(t)]/2$. Technically there is an additional important aspect to consider. The magneto-optical response is in principle related to the nondiagonal part of the dielectric tensor (ε_{ij}, $i \neq j$) while the optical response is given by the diagonal part of the tensor (ε_{ii}, $i = x,y,z$). In the dynamics, ε_{ij} also depends on $\Delta R(t)$ and $\Delta T(t)$ but these two quantities are two orders of magnitude smaller than the magnetic rotation $\Delta\theta(t)$ as seen for example in Fig. 3(a), where the normalized quantities $\Delta R(t)/R$ and $\Delta\theta(t)/\theta_s$ are plotted. θ_s is the static magneto-optical Kerr rotation. The spot sizes and the energy densities of the pump and the probe were about 130 and 50 μm in diameter and 1.5 mJ/cm^2 and 1.3 μJ/cm^2, respectively. The freestanding Ni films (6×6 mm^2) are obtained by using sodium chloride as a sacrificial layer

*jean-yves.bigot@unistra.fr

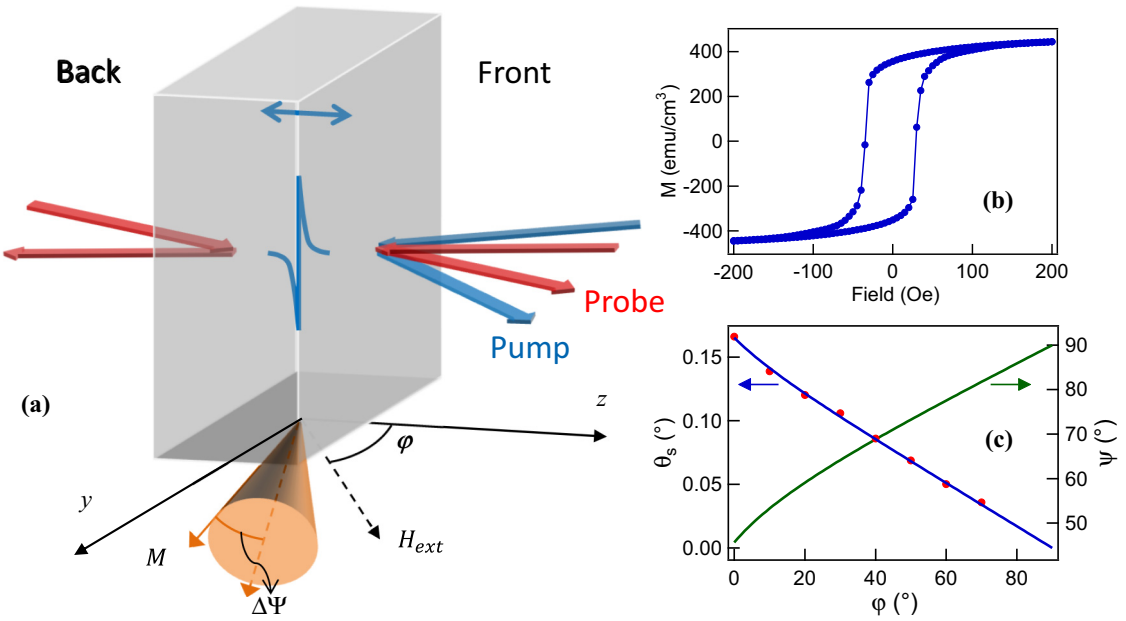

FIG. 1. Experimental setup and characterization of the Ni freestanding film. (a) Sketch of the freestanding film cavity experiment. (b) Magnetization curve of the freestanding Ni film. (c) Magneto-optical polar Kerr angle $\theta_s(\varphi)$ obtained from experimental data (solid circles) on the left axis and equilibrium angle $\Psi(\varphi)$ of the effective field on the right axis.

between Ni and a glass substrate. After Ni deposition, we soak the sample in water to dissolve the sacrificial layer and transfer the freestanding film to the sample holder with a hole. As the elastic and magnetoelastic properties of the film should be well-defined for the acoustic pulse propagation and magnetization dynamics, we stretched the film laterally as much as possible by gluing a silver paste around the edges of the film. To control the period of the magnetization precession, we varied the angle φ of the external magnetic field $H_{\text{ext}} = 0.4\,\text{T}$, defined with respect to the z axis (normal to the sample). Figure 1(c) presents the equilibrium angle Ψ of the effective field axis as a function of φ. For that purpose, we fitted the polar Kerr rotation angles $\theta_s(\varphi)$ measured experimentally (solid circles) with the free-energy equation $F = (K + \mu_0 M_s^2/2)\cos^2\Psi - \mu_0 H_{\text{ext}} M_s \cos(\Psi - \varphi)$. Since the elastic stiffness, and accordingly the magnetocrystalline anisotropy coefficient K, can yield different values from the one of the bulk due to the stress induced by the silver paste, we set the magnetic anisotropy coefficient K as a free parameter. The magnetization at saturation ($M_s = 480\,\text{emu/cm}^3$) is obtained from the hysteresis measurement of Fig. 1(b).

Figure 2(a) shows the magnetization precession angle dynamics $\Delta\Psi(t)$ (left axis) at several angles φ and the transient reflectivity $\Delta R(t)/R$ (right axis) measured at the back side of the film. The time scale represents the absolute time t with the definition of $t = 0$ corresponding to the arrival of the femtosecond pump pulse at the FS of the sample. For the magnetization precession curves influenced by acoustic echoes, in the only condition that $T_{ac} = hT_{\text{prec}}$ (T_{ac}: a round trip time of acoustic pulse, T_{prec}: a period of precession, h: a positive integer), its precession amplitude is added up in phase. Otherwise, the precession phase cannot be maintained and the amplitude decreases. The curves measured at $\varphi = 15.5°$ and 65° correspond to $h = 1$ and 2, and one can see that their amplitudes increase along the acoustic echoes with phases unchanged. Regarding the decrease of the amplitude after several round trips, it is due to the fact that the energy gain from echoes does not overcome the energy dissipation from the magnetization damping. Although the acoustic pulse is expected to be mostly reflected at Ni/air interfaces, the amplitudes of the echoes, as appearing in the top curve of Fig. 2(a), are attenuated and dispersed. We will discuss this further when considering Fig. 4. For the other angles $\varphi = 26°$ and 46.5°, the phases of the precession change due to the echoes and therefore amplitudes cannot increase. At the intermediate angle $\varphi = 35°$ ($h = 3/2$), the echoes repeatedly suppress the precession. We can see these aspects in the fast Fourier transform (FFT) spectra obtained after removing the slow-varying background signal as shown in Fig. 2(b). The magnetization precession is maintained at the frequency-matching condition of spectral lines of $\Delta R(t)/R$ [Fig. 2(b1)] and $\Delta\Psi(t)$ [Fig. 2(b2)]. This occurs for the resonant conditions ~9.8, 19.5, 29.3, ... GHz of the frequency comb related to the acoustic echoes [Fig. 2(b1)]. The beatinglike behavior showing two frequencies in Fig. 2(b2) is the result of the suppression of the precession when the round-trip time T_{ac} is mismatched with T_{prec}. Indeed, the estimation of a beating frequency between the first-order and uniform modes ($\Delta f = f_1 - f_0$) is ~0.1 GHz (10 ns), using a spin-wave exchange constant of 430 meV Å^2 [22]. This is much different than both the damping time and the time window of our measurements. There is no other mode except the uniform mode which could be attributed for example to phonons and magnons.

In order to obtain information about how long the acoustic echoes influence the magnetization precession, we model $\Delta\Psi(t)$ by

$$\Delta\Psi(t)/\Delta\Psi(0) = e^{-t/\xi_1}\cos(\omega t + \varsigma) \times\left[1 + \sum_m q(m)\,\Theta(t - mT_{\text{prec}})\right], \quad (1)$$

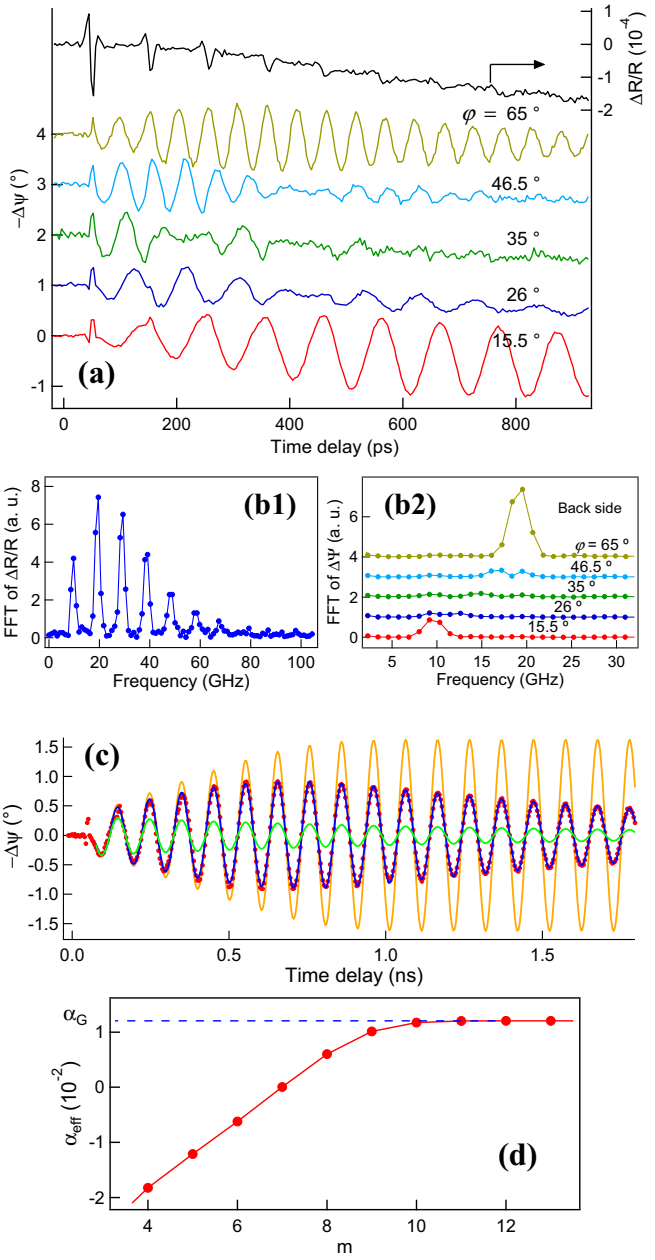

FIG. 2. Magnetization dynamics on the back side of the Ni film. (a) Magnetization precession angle dynamics $\Delta\Psi(t)$ (left axis) for several angles φ and transient reflectivity $\Delta R(t)/R$ (right axis) measured at the back side of the freestanding film. (b) Fourier transform of reflectivity (b1) and Kerr rotation (b2) obtained from Fig. 2(a). (c) Long delay scan for $\varphi = 15.5^\circ$ (solid circles) and model fit curves (green, orange, and blue curves: the magnetization precession associated with the Gilbert intrinsic damping α_G, extrinsic damping α_{ext}, and effective damping α_{eff}, respectively). (d) Gilbert effective damping α_{eff} with a function of the order of acoustic echoes, extracted from the model fit.

where ξ_1 is a damping time related to the Gilbert intrinsic damping α_G by $1/\omega\xi_1$, ζ is a constant phase factor, Θ is the Heaviside function, and $q(m)$ is a function that takes into account the decrease of the echo amplitude of order m which tends to zero for large orders $[q(m) \underset{m\geqslant M}{\mapsto} 0]$. We used the trial function $q(m) \propto e^{-(mT_{\text{prec}}/\xi_2)^{\nu}}$, where $\xi_2(= 690\,\text{ps})$ and $\nu(= 4.2)$ are fitting parameters associated with the amplitudes of the echoes. After fitting $\Delta\Psi(t)$ $(h = 1)$ with the above model, which is governed by the Gilbert effective damping α_{eff} [blue curve in Fig. 2(c)], we obtain both the Gilbert intrinsic damping α_G and extrinsic damping α_{ext} which reflects the energy gain from the acoustic echoes. They are presented with green and orange curves, respectively, in Fig. 2(c). For the orange curve, the amplitude of the magnetization precession increases due to the repeated excitation of the acoustic echoes and becomes saturated after the attenuation of acoustic echoes. At this point, the Gilbert effective damping α_{eff} $(= \alpha_G + \alpha_{\text{ext}})$ converges to the intrinsic damping α_G, the variation of which is presented in Fig. 2(d). Here, we obtain $\alpha_G = 0.012$ irrespective of the order of echoes for $m \geqslant 12$. In addition, by comparing the blue and green curves, we obtain the amplifying factor 4.5 for the acoustic echoes in this freestanding film. Empirically, we found that the properties of an acoustic pulse after generation, propagation, and reflection were dependent on the static lateral tensile (longitudinal compressive) stress exerted on the freestanding film, that is, the higher the stress, the larger the acoustic pulse and the less the loss, although we could not quantify that in this paper. In the results presented here the lateral stress is such that the echoes survive up to 12 round trips.

Our experimental configuration also allows us to simultaneously retrieve information about the dynamics of the magnetization precession occurring on the FS of the sample. Figure 3(a) shows $\Delta\theta(t)/\theta_s$ (left axis) for various angles φ after subtracting the thermal magnon background and $\Delta R(t)/R$ (right axis) on the FS of the sample. For temporal delays up to ~300 ps, we find that the magneto-optical signals are different from those from the BS of sample in terms of their precession frequencies and phases. Correspondingly, in Fig. 3(b) two curves $\Delta\theta(t)/\theta_s$ (left axis, open circles, FS of sample) and $\Delta\Psi(t)$ (right axis, closed circles, BS of sample) for $\varphi = 15.5^\circ$ are shown, where $\Delta\Psi(t)$ has been forward shifted by $T_{ac}/2$ so that both magnetization trajectories are compared on the same local temporal scale associated with the FS of the sample. Since there is obviously a strong perturbation of the phase in the FS of the sample, we introduce the concept of time-dependent frequency $f_{FS}(t)$, well known in the theory of signal when there is a time-dependent drift of the main resonance frequency. This results in an asymmetry of the FFT spectra as shown in Fig. 3(c) represented in log scale. The asymmetry in the FS spectrum as compared to the BS shows up for low frequencies. In contrast, the spectrum from the BS of the sample signal is symmetric and the frequency $f_{BS}(t)$ is almost constant. To better show the time evolution of the precession frequency on the FS we plot in the inset of Fig. 3(b) the temporal difference ΔT between the two precession signals as a function of the echo order m. ΔT displays a nonlinear increase and converges to a nonzero positive value (~8 ps).

Let us now explain the origin of the phase temporal drift $\Delta T(t)$ in the magnetization precession at the FS of the sample as compared to the BS. It results from the repetitive excitation of the magnetization by the acoustic echoes which have opposite directions at FS and BS. Indeed, because of the propagation directions, the compressive and tensile parts of the

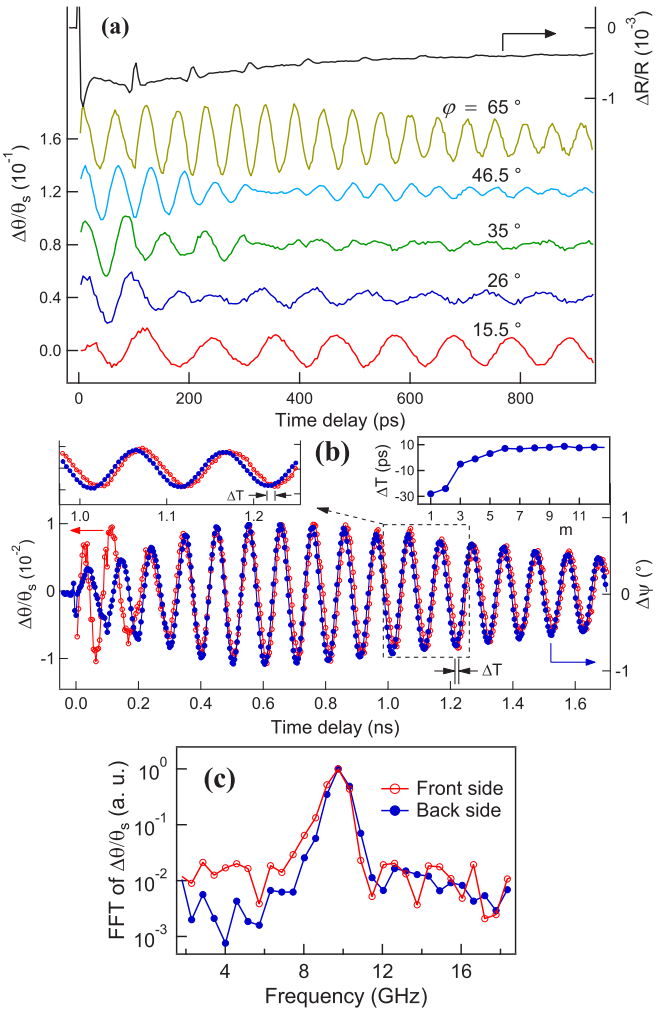

FIG. 3. Magnetization dynamics on the front side compared to the back side. (a) Magnetization precession dynamics $\Delta\theta(t)/\theta_s$ (left axis) for several angles φ and transient reflectivity $\Delta R(t)/R$ (right axis) measured at the front side of the freestanding film. (b) Comparison between the front- and back-sides' temporal responses of the magnetization precession for $\varphi = 15.5°$. The open and solid circles represent the front-side data on the left axis and back-side data on the right axis, which is forward shifted by $T_{ac}/2$. The inset on the top left shows a magnified view of the precession and the definition of the phase shift ΔT. The inset on the top right shows the evolution of the temporal different ΔT between two precession curves as a function of the echo order m. (c) Fourier transforms of the front- and back-side precession for the same conditions as Fig. 3(b). Note the log scale.

strains are reversed. Therefore at FS each echo induces a "kick" directed along $-Oz$ [see Fig. 1(a)] while it is along $+Oz$ at BS. With our conventions, when the static field H_{ext} points along $+Oz$ (magnetization pointing inward of the sample at BS) and if $T_{ac} = T_{\text{prec}}$, then the precession at BS is amplified and no phase is added at each echo as seen in closed circles in Fig. 3(b) (recall that the precession curve has been shifted by $T_{ac}/2$ for the sake of comparison with the FS precession motion). In contrast, at the FS the magnetization initially points outward of the sample and starts precessing due to the laser-induced thermal effect. But, the first two echoes propagating along $+Oz$ are enough to reverse the phase of the precession, the motion of which now becomes π-shifted with respect to the BS. After a few acoustic echoes, the FS precession does not change much as the amplitudes of the remaining echoes are small. The time-dependent frequency $f_{FS}(t)$, or equivalently ΔT, varies rapidly and then stabilizes to a plateau which is slightly positive [+8 ps in the right inset of Fig. 3(b)] because of the mismatch between T_{ac} and T_{prec}. This analysis can be directly inferred from a preceding detailed work performed on Ni/Al_2O_3 perturbed by a sequence of acoustic pulses [23].

We stress that, in addition to the phase shift due to the repetitive action of the acoustic echoes, one has to consider on the FS of the sample the reduction of the magnetization modulus due to the thermal heating. It can be described by the Landau-Lifshitz equations coupled to the two-temperature model [24]. A detailed study, performed on Co thin films with different anisotropies, could show that the interplay between the change of modulus, which vanishes at the Curie temperature, and the temperature-dependent magnetocrystalline anisotropy, strongly modifies the magnetization trajectory. This mechanism is however most important during the first picosecond before the spin temperature gets in equilibrium with the one of the lattice.

Let us now focus on the change of the temporal profile of the acoustic pulses while propagating in the freestanding film. It is important because, as seen in Fig. 2(a), the amplitude of the acoustic echoes decreases while its temporal width increases simultaneously. As a reference we will compare it to the one of acoustic pulses propagating in a Ni (290 nm) deposited on a glass substrate by electron-beam evaporation. For a better characterization of the acoustic pulses, we reconstruct the time-dependent strain profile $\eta(t)$ from the experimental data and perform a Fourier analysis. From the experimental reflectivity $\Delta R(t)/R$, and using equations described in Ref. [25], we obtain

$$\eta(t) = \frac{\lambda}{16\pi^2 \upsilon} \int_{-\infty}^{\infty} \frac{\Delta\tilde{R}(\omega)}{R} \tilde{G}(\omega)^{-1} e^{i\omega t} d\omega, \qquad (2)$$

where $\lambda = 800\,\text{nm}$, $\upsilon = 5.9\,\text{nm/ps}$. $\Delta\tilde{R}(\omega)/R$ and $\tilde{G}(\omega)$ are Fourier transforms of the measured reflectivity signal $\Delta R(t)/R$ and the response function $G(t)$ defined as follows:

$$G(t) = [\chi' \sin(\omega' t) + \chi'' \cos(\omega' t)\,\text{sign}(t)] e^{-\omega''|t|}. \qquad (3)$$

As the refractive index ($\tilde{n} = 2.48 + 4.38i$) and the photoelastic coefficient ($\partial\tilde{n}/\partial\eta = 0.6 - 1.8i$) at $\lambda = 800\,\text{nm}$ are known [26,27], the coefficients which we used here are given by $\chi' + i\chi'' = 2\tilde{n}(\partial\tilde{n}/\partial\eta)/(1-\tilde{n}^2)$ and $\omega' + i\omega'' = 4\pi\upsilon\tilde{n}/\lambda$. We avoid the singularity of $\tilde{G}(0)$ by taking $\Delta\tilde{R}(0) = 0$ after eliminating the background offset signal in the time domain. Through a straightforward calculation using the experimental $\Delta R(t)/R$ of the echoes in the front side, the strain profiles of echoes of order m $\eta_m(t)$ and $\tilde{\eta}_m(\omega)$ are reconstructed in Figs. 4(a) and 4(b), respectively. For comparison, in the case of the Ni/SiO_2 film, the corresponding reconstructed $\eta_m(t)$ and $\tilde{\eta}_m(\omega)$ profiles are shown in Figs. 4(c) and 4(d). From these sets of figures, we see that $\eta_m(t)$ of the freestanding film is broader than that of Ni/SiO_2. This broadening as well as the attenuation of the strain profiles persists as m increases.

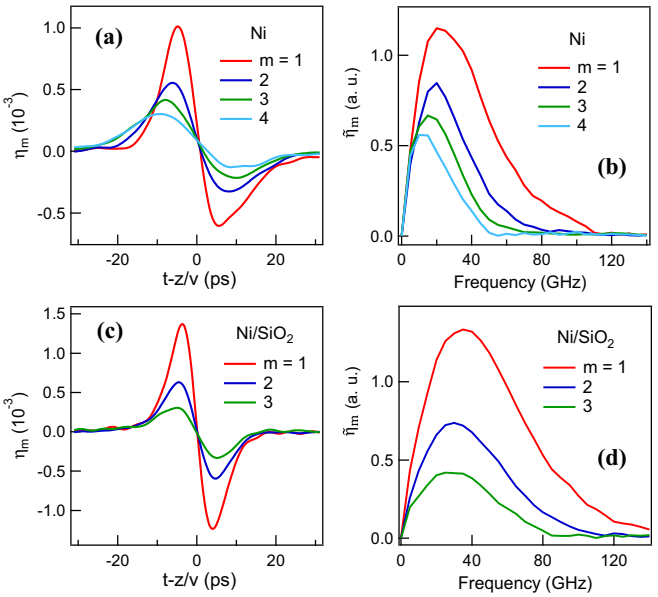

FIG. 4. Strain profiles in Ni and Ni/SiO_2. (a) and (c) Reconstructed strain profiles of echoes in the time domain $\eta_m(t)$ for the freestanding Ni and Ni/SiO_2, respectively. (b) and (d) Strain profiles of echoes in the frequency domain $\tilde{\eta}_m(\omega)$ for each film.

Although the main contribution to the attenuation of acoustic pulses is a transmission loss at a film/substrate interface (acoustic reflection coefficient $r_{ac} \sim 0.54$ for Ni/SiO_2), the freestanding Ni with $r_{ac} \sim 1$ has an abnormally large attenuation. Practically, r_{ac} is not equal to 1 but instead is frequency dependent due to the roughness and the inhomogeneity of the thickness within the beam size as described in the case of membrane [28]. However, in the present study the metallic deposition process is similar for both samples (freestanding Ni and Ni/SiO_2) and the spot diameters of the pumps are also the same. To check the quality of our reference film as compared to the one of bulk Ni, we extract the frequency-dependent attenuation term $\alpha(\omega)$ which reflects the internal properties of a film such as dislocation, defect, stacking fault, porosity, and grain boundary [29]. $\alpha(\omega)$ can be applied to $\tilde{\eta}_m(\omega)$ for the next echo $\tilde{\eta}_{m+1}(\omega)$ using the following equation:

$$\alpha(\omega) = \alpha_0 \left(\frac{\omega}{2\pi}\right)^{\beta} = \frac{1}{2d} \ln \frac{r_{ac}\tilde{\eta}_m(\omega)}{\tilde{\eta}_{m+1}(\omega)}, \tag{4}$$

where d (290 nm) is the film thickness of Ni/SiO_2, α_0 is the frequency-independent coefficient, and β is an exponent in the power-law relation, the value of which is 2 as known for Ni [30] and other materials [31,32]. Using a least-square fitting, we obtained the value 0.10 Np ps^2/nm for α_0, which is comparable to values of polycrystalline Ni films deposited on a quartz substrate [33]. Therefore we conclude that the large attenuation present in the freestanding Ni film as compared to the reference Ni/SiO_2 sample is not related to the quality of the film either in the bulk or at the surface.

Although Fig. 4 obviously shows that the attenuation and dispersion of the freestanding Ni film are much larger than those of the reference film, it is not possible to compare the values of α_0 directly because β may vary due to various scattering mechanisms of phonons [28,34,35]. For a film deposited on a substrate, the lateral stress due to the lattice mismatch and the different thermal expansion coefficients of the film and the substrate is different from that of the freestanding film. Therefore it is important to study the effect of the stress dependence on the attenuation. To the best of our knowledge, the effect of temperature on attenuation has been studied relatively well [31,36,37]. In contrast the effect of stress has been studied for crystalline bulk systems [38,39] but not for films. It is essential to investigate the change of both the speed and the temporal profile of an acoustic pulse while varying the thickness of a bulk down to the one of deposited thin films. Alternatively, one can quantitatively control the lateral stress of a film using a piezoelectric substrate as it would modify the speed of the acoustic pulse through nonzero third-order elastic tensors [40–42] associated with the attenuation [43]. This approach would allow us to make an important connection between attenuation and stress for a freestanding film and to develop a simple design of an acoustic cavity. This is an interesting research subject to be explored beyond the scope of the present study.

In conclusion, we have investigated the characteristics of acoustic pulses and magnetization dynamics in a freestanding Ni film behaving as an acoustic cavity. Due to the multiple round trips of echoes, the amplitude of the magnetization precession is enhanced by a factor of 4.5. The comparison of the magnetization precession on both sides of the sample allows us to explain the phase dynamics of the precession oscillations. In addition, we found that the acoustic pulses in the cavity display much larger attenuation compared with a reference sample Ni/SiO_2 and they nearly disappear after 12 round trips. We conjecture that this behavior is due to lateral stress, which is removed in the freestanding film. Undoubtedly, a systematic study of the relation between external stress and attenuation, which so far remains unexplored, would give important information for realizing efficient acoustic cavities based on freestanding films. Also, our results are important for designing acoustic cavities displaying a large amplification of the magnetization precession angle and ultimately leading to the nonlinear regime of the precession dynamics [44] as well as the precession-based magnetization reversal [15].

The authors acknowledge the financial support of the Agence Nationale de la Recherche in France via the project EQUIPEX UNION: No. ANR-10-EQPX-52.

[1] E. Beaurepaire, J.-C. Merle, A. Daunois, and J.-Y. Bigot, Phys. Rev. Lett. **76**, 4250 (1996).
[2] C. Thomsen, J. Strait, Z. Vardeny, H. J. Maris, J. Tauc, and J. J. Hauser, Phys. Rev. Lett. **53**, 989 (1984).
[3] H.-Y. Hao and H. J. Maris, Phys. Rev. Lett. **84**, 5556 (2000).
[4] O. L. Muskens and J. I. Dijkhuis, Phys. Rev. Lett. **89**, 285504 (2002).

[5] S. Tamura, D. C. Hurley, and J. P. Wolfe, Phys. Rev. B **38**, 1427 (1988).

[6] A. Yamamoto, T. Mishina, Y. Masumoto, and M. Nakayama, Phys. Rev. Lett. **73**, 740 (1994).

[7] T. Czerniuk, C. Brüggemann, J. Tepper, S. Brodbeck, C. Schneider, M. Kamp, S. Höfling, B. A. Glavin, D. R. Yakovlev, A. V. Akimov, and M. Bayer, Nat. Commun. **5**, 4038 (2014).

[8] T. Dehoux, M. Abi Ghanem, O. F. Zouani, J.-M. Rampnoux, Y. Guillet, S. Dilhaire, M.-C. Durrieu, and B. Audoin, Sci. Rep. **5**, 8650 (2015).

[9] A. V. Akimov, A. V. Scherbakov, D. R. Yakovlev, C. T. Foxon, and M. Bayer, Phys. Rev. Lett. **97**, 037401 (2006).

[10] A. V. Scherbakov, A. S. Salasyuk, A. V. Akimov, X. Liu, M. Bombeck, C. Brüggemann, D. R. Yakovlev, V. F. Sapega, J. K. Furdyna, and M. Bayer, Phys. Rev. Lett. **105**, 117204 (2010).

[11] J.-W. Kim, M. Vomir, and J.-Y. Bigot, Phys. Rev. Lett. **109**, 166601 (2012).

[12] M. Bombeck, A. S. Salasyuk, B. A. Glavin, A. V. Scherbakov, C. Brüggemann, D. R. Yakovlev, V. F. Sapega, X. Liu, J. K. Furdyna, A. V. Akimov, and M. Bayer, Phys. Rev. B **85**, 195324 (2012).

[13] V. V. Temnov, Nat. Photonics **6**, 728 (2012).

[14] O. Kovalenko, T. Pezeril, and V. V. Temnov, Phys. Rev. Lett. **110**, 266602 (2013).

[15] L. Thevenard, J.-Y. Duquesne, E. Peronne, H. J. von Bardeleben, H. Jaffres, S. Ruttala, J.-M. George, A. Lemaître, and C. Gourdon, Phys. Rev. B **87**, 144402 (2013).

[16] K. Shinokita, K. Reimann, M. Woerner, T. Elsaesser, R. Hey, and C. Flytzanis, Phys. Rev. Lett. **116**, 075504 (2016).

[17] J. V. Jäger, A. V. Scherbakov, B. A. Glavin, A. S. Salasyuk, R. P. Campion, A. W. Rushforth, D. R. Yakovlev, A. V. Akimov, and M. Bayer, Phys. Rev. B **92**, 020404(R) (2015).

[18] F. Hudert, A. Bruchhausen, D. Issenmann, O. Schecker, R. Waitz, A. Erbe, E. Scheer, T. Dekorsy, A. Mlayah, and J.-R. Huntzinger, Phys. Rev. B **79**, 201307(R) (2009).

[19] A. Bruchhausen, R. Gebs, F. Hudert, D. Issenmann, G. Klatt, A. Bartels, O. Schecker, R. Waitz, A. Erbe, E. Scheer, J.-R. Huntzinger, A. Mlayah, and T. Dekorsy, Phys. Rev. Lett. **106**, 077401 (2011).

[20] M. Schubert, M. Grossmann, C. He, D. Brick, P. Scheel, O. Ristow, V. Gusev, and T. Dekorsy, Ultrasonics **56**, 109 (2015).

[21] M. Trigo, A. Bruchhausen, A. Fainstein, B. Jusserand, and V. Thierry-Mieg, Phys. Rev. Lett. **89**, 227402 (2002).

[22] M. van Kampen, C. Jozsa, J. T. Kohlhepp, P. LeClair, L. Lagae, W. J. M. de Jonge, and B. Koopmans, Phys. Rev. Lett. **88**, 227201 (2002).

[23] J.-W. Kim, M. Vomir, and J.-Y. Bigot, Sci. Rep. **5**, 8511 (2015).

[24] J.-Y. Bigot, M. Vomir, L. H. F. Andrade, and E. Beaurepaire, Chem. Phys. **318**, 137 (2005).

[25] K. J. Manke, A. A. Maznev, C. Klieber, V. Shalagatskyi, V. V. Temnov, D. Makarov, S.-H. Baek, C.-B. Eom, and K. A. Nelson, Appl. Phys. Lett. **103**, 173104 (2013).

[26] P. B. Johnson and R. W. Christy, Phys. Rev. B **9**, 5056 (1974).

[27] T. Saito, O. Matsuda, and O. B. Wright, Phys. Rev. B **67**, 205421 (2003).

[28] J. Cuffe, O. Ristow, E. Chávez, A. Shchepetov, P.-O. Chapuis, F. Alzina, M. Hettich, M. Prunnila, J. Ahopelto, T. Dekorsy, and C. M. Sotomayor Torres, Phys. Rev. Lett. **110**, 095503 (2013).

[29] A. S. Nowick and B. S. Berry, *Anelastic Relaxation in Crystalline Solids* (Academic, New York, 1972).

[30] M. Gupta, M. Wan, S. K. Verma, and R. R. Yadav, Ultrasonics **54**, 2115 (2014).

[31] J.-Y. Duquesne and B. Perrin, Phys. Rev. B **68**, 134205 (2003).

[32] R. K. Singh, R. P. Singh, M. P. Singh, and P. C. Srivastava, J. Phys.: Condens. Matter **20**, 345227 (2008).

[33] W. Sigle and W. Weis, Z. Phys. B: Condens. Matter **53**, 75 (1983).

[34] C. Herring, Phys. Rev. **95**, 954 (1954).

[35] G. L. Guthrie, Phys. Rev. **152**, 801 (1966).

[36] B. C. Daly, K. Kang, Y. Wang, and D. G. Cahill, Phys. Rev. B **80**, 174112 (2009).

[37] G. Baldi, V. M. Giordano, B. Ruta, R. Dal Maschio, A. Fontana, and G. Monaco, Phys. Rev. Lett. **112**, 125502 (2014).

[38] N. K. Gobran and H. Youssef, J. Phys. C: Solid State Phys. **3**, S24 (1970).

[39] V. V. Kozhushko, G. Paltauf, H. Krenn, S. Scheriau, and R. Pippan, J. Appl. Phys. **107**, 094905 (2010).

[40] R. N. Thurston and K. Brugger, Phys. Rev. **133**, A1604 (1964).

[41] Y. Hiki and A. V. Granato, Phys. Rev. **144**, 411 (1966).

[42] T. Çağin and B. M. Pettitt, Phys. Rev. B **39**, 12484 (1989).

[43] W. P. Mason and T. B. Bateman, J. Acoust. Soc. Am. **40**, 852 (1966).

[44] C. A. Perroni and A. Liebsch, J. Phys.: Condens. Matter **18**, 7063 (2006).